THE ASTROPHYSICAL JOURNAL, **266**:287–297, 1983 March 1

THE MASS OF TYCHO'S SUPERNOVA REMNANT AS DETERMINED FROM A HIGH-RESOLUTION X-RAY MAP

F. SEWARD, P. GORENSTEIN, AND W. TUCKER
Harvard-Smithsonian Center for Astrophysics
Received 1982 June 18; accepted 1982 August 26

ABSTRACT

The *Einstein* high-resolution image of Tycho's supernova remnant clearly shows hot material behind a shock propagating into the interstellar medium at the outer edge of the remnant. The morphology of the remnant is not far from numerical results predicting a strong reverse shock. The reverse-shocked material that we observe, however, has broken into clumps and spread radially so this inner shell of emission is thicker than predicted.

A model is developed which distinguishes between the shocked interstellar material and the ejecta which are visible as bright patches behind the shock. The picture is analyzed to derive the mass of X-ray emitting material. Assuming a distance of 3 kpc, an absorbing column density of 3×10^{21} atoms cm^{-2}, and using a nonequilibrium calculation for the emissivity, we find the average density of the ISM is 0.4 atoms cm^{-3}, and the energy contained in the remnant is 1.4×10^{51} ergs. The total mass of X-ray emitting material in the remnant is $\approx 4\ M_\odot$, $\approx 2\ M_\odot$ ejecta, and $\approx 2\ M_\odot$ swept-up, putting the remnant at an intermediate state between a free expansion and the Sedov phase.

Subject headings: interstellar: matter — nebulae: supernova remnants — shock waves — X-rays: sources

I. INTRODUCTION

In the study of the evolution of supernova remnants and the nature of the supernova explosion itself, Tycho's remnant occupies a unique and important position. Since the remnant is undoubtedly associated with the supernova observed in 1572 (Clark and Stevenson 1977), the age of the remnant is known. The light curve was well measured (Baade 1945) and firmly establishes the supernova as type I. Indeed, when a "typical" example of a type I supernova is mentioned in the literature, it is usually Tycho's. Information concerning the mass of ejecta in this SNR are therefore vital to determining the nature of the type I supernova explosion.

Much of the recent theoretical work has centered on low mass stars as progenitors of Type I supernova. A number of authors (Arnett 1979; Chevalier 1981; Nomoto 1981; Wheeler 1982) have considered accreting white dwarfs of $\sim 1.5\ M_\odot$ which are disrupted completely by the explosion, leaving no compact remnant and producing a large amount of ^{56}Ni. In a more general way, Lasher (1975) showed that the narrowness of the peak of the early Type I supernova light curve required $\lesssim 2\ M_\odot$ of ejecta. This is consistent with the observed lack of correlation of Type I supernovae with spiral arms which points to an older stellar population of low-mass stars (see, e.g., Maza and van den Bergh 1976).

On the other hand, Oemler and Tinsley (1979) have argued that Type I supernovae are correlated with star formation rates and are therefore associated with stars having lifetimes less than about a billion years, or masses greater than about two solar masses. Weaver, Axelrod, and Woosley (1980) have shown how the evolution of a 9 $M_\odot$ star can lead to a Type I supernova event consistent with the observations. So, the question as to the mass of the progenitor remains open.

Another approach to this problem is to study the dynamics of the remnant. Strom, Goss, and Shaver (1982) have recently made an important contribution in this connection. Using two radio maps taken 8 years apart, they have shown that the expansion velocity of Tycho's SNR is 3600 ± 360 km s^{-1} at a radius of 221″ or 0.99×10^{19} cm, assuming a distance of 3 kpc. This is to be compared with the average velocity of expansion which is 7640 km s^{-1} over the 410-year lifetime of Tycho's SNR. The ratio of the present to the average velocity is 0.47 ± 0.044, in agreement with the results of Kamper and van den Bergh (1976) which were based on optical observations.

These results have generally been taken as proof that Tycho's supernova remnant is in the adiabatic phase, with the swept-up mass much greater than the ejected mass. In this phase the radius $R \propto t^{2/5}$, so the velocity $\dot{R} = V = 2/5(R/t) = 0.4\bar{V}$. However, a comparison of the instantaneous and average velocities of expansion may be misleading if a reverse shock (McKee 1974) is present. The reverse shock, moving back into the expanding ejecta, appears to an external observer to be expanding at a lower velocity than the primary shock propagating into the interstellar medium (ISM). If the reverse shock is bright, the observed expansion will be closer to that of the reverse shock than that of the shock in the ISM.

Yet another approach is to attempt to infer the mass by means of X-ray observations. The observed morphology, a model for the three-dimensional structure, and the measured X-ray surface brightness and temperature can be used to calculate the amount of X-ray emitting plasma.

Spectra taken with the *Einstein* SSS (Becker *et al.* 1980) show surprinsingly strong emission lines, particularly from Si and S. Both equilibrium and nonequilibrium models require several times solar abundance of Si group elements (Shull 1982*a*). The spectrum obtained from *HEAO 1* (Pravdo *et al.* 1980) shows X-ray emission to at least 25 keV, requiring high temperatures in at least part of the remnant.

An *Einstein* IPC observation presented by Reid, Becker, and Long (1982) gives the same picture as the HRI observation to be discussed here but with more emphasis on X-rays of a few keV energy and with lower spatial resolution. They derive a mass of X-ray emitting material of 15 $M_\odot$ and a density of 2.3 atoms cm^{-3} for the ISM, typical of past results for this remnant. The better resolution of the HRI, a lower ISM column density, and a nonequilibrium emissivity calculation lead to an ISM density of only 0.4 (this paper). These factors also lead to a lower calculated mass of the remnant. The X-ray luminosity is consistent with this lower mass because of high emissivity from nonequilibrium effects and enrichment of metal abundances.

The high-resolution *Einstein* data have been compared to radio maps by Dickel, Murray, and Morris (1982) to show the bulk of the radio and X-ray emission to be from a shell with a thickness about one-fourth the radius. Van den Bergh, Marscher, and Terzian (1973) give an optical picture of the remnant showing faint filaments around the outer edge of the northern half. The position of these filaments relative to the X-ray and radio emission is discussed by Reid *et al.* and by Dickel *et al.* Further comparison with radio and optical data is outside the scope of this paper.

In the following sections, we will show that the high-resolution *Einstein* image has features which can be interpreted as a shock heated shell in the ISM and an inner shell containing ejecta which has broken into clumps. The mass of plasma in each region will be calculated from the observed surface brightness using emissivities generated from a model in which ions and electrons are not in equilibrium. The result places the remnant in a phase intermediate between a free expansion and the Sedov phase.

II. PAST OBSERVATIONS AND RESULTS FOR A SIMPLE MODEL

Table 1 lists some past X-ray observations of Tycho's SNR. Early detections are not included. Each of the observations listed resulted in a fairly good low-resolution spectral measurement from which the X-ray luminosity, L_X, could be calculated. We have listed both the results quoted in the original papers and results obtained by us using the same plasma temperature, T, and absorption in the ISM, column density = N_H, for each observation. The present HRI data are included for comparison. Numbers in square brackets have been calculated by us as have all items in the fourth and following rows.

Even after removing the variation caused by differing estimates of temperature and column density (which has been particularly difficult to measure using the X-ray spectra), the calculated L_X follows the measured X-ray flux and varies a factor of 3. The value of L_X quoted by Reid *et al.* is high because of the assumed low T and large N_H. That derived from the data of Pravdo *et al.* is high because of a high flux determination and a moderate column density.

Once the luminosity is known, a simple model is used to derive the mass. The remnant is assumed to be a uniform spherical shell with thickness = one-fifth the radius. Distance is 3 kpc. The radius is that of the radio shell, 220″. Plasma is in equilibrium. Abundances of elements are assumed to be cosmic (≈ solar) for these comparative mass estimates.

These results show that it has been difficult to measure the incident X-ray flux, and that derived L_X and mass are particularly sensitive to the assumed column density of absorbing material. The "simple" model mass we derive from the *Einstein* HRI data is also subject to these

TABLE 1

X-RAY OBSERVATIONS OF TYCHO'S SUPERNOVA REMNANT

Observers	0.2–4 keV Flux at Detector (ergs cm^{-2} s^{-1})	T and N_H (keV) (atoms cm^{-2})	0.2–4 keV Flux Corrected for Absorption (ergs cm^{-2} s^{-1})	L_X 3 kpc (ergs s^{-1})	M ($M_\odot$)
Hill *et al.* 1975	5.2 (−10)	2, 8 (20)	8.6 (−10)	9.2 (35)	[13]
Pravdo *et al.* 1980	1.2 (−9)	0.7, 6, 8 (21)	...	[7.2 (36)]	[26]
Reid *et al.* 1981	...	0.45, 1.6 (22)	4.9 (−9)	5.3 (36)	21
Hill *et al.* 1975	5.2 (−10)	1, 3 (21)	...	1.1 (36)	11
Pravdo *et al.* 1980	1.2 (−9)	1, 3 (21)	...	2.6 (36)	16
Einstein IPC[a]	3.4 (−10)	1, 3 (21)	...	7.4 (35)	9
Einstein HRI[b]	2.6 (−10)	1, 3 (21)	...	5.5 (35)	7

[a] Data of Reid *et al.* 1981.

[b] Data of this paper with simple analysis.

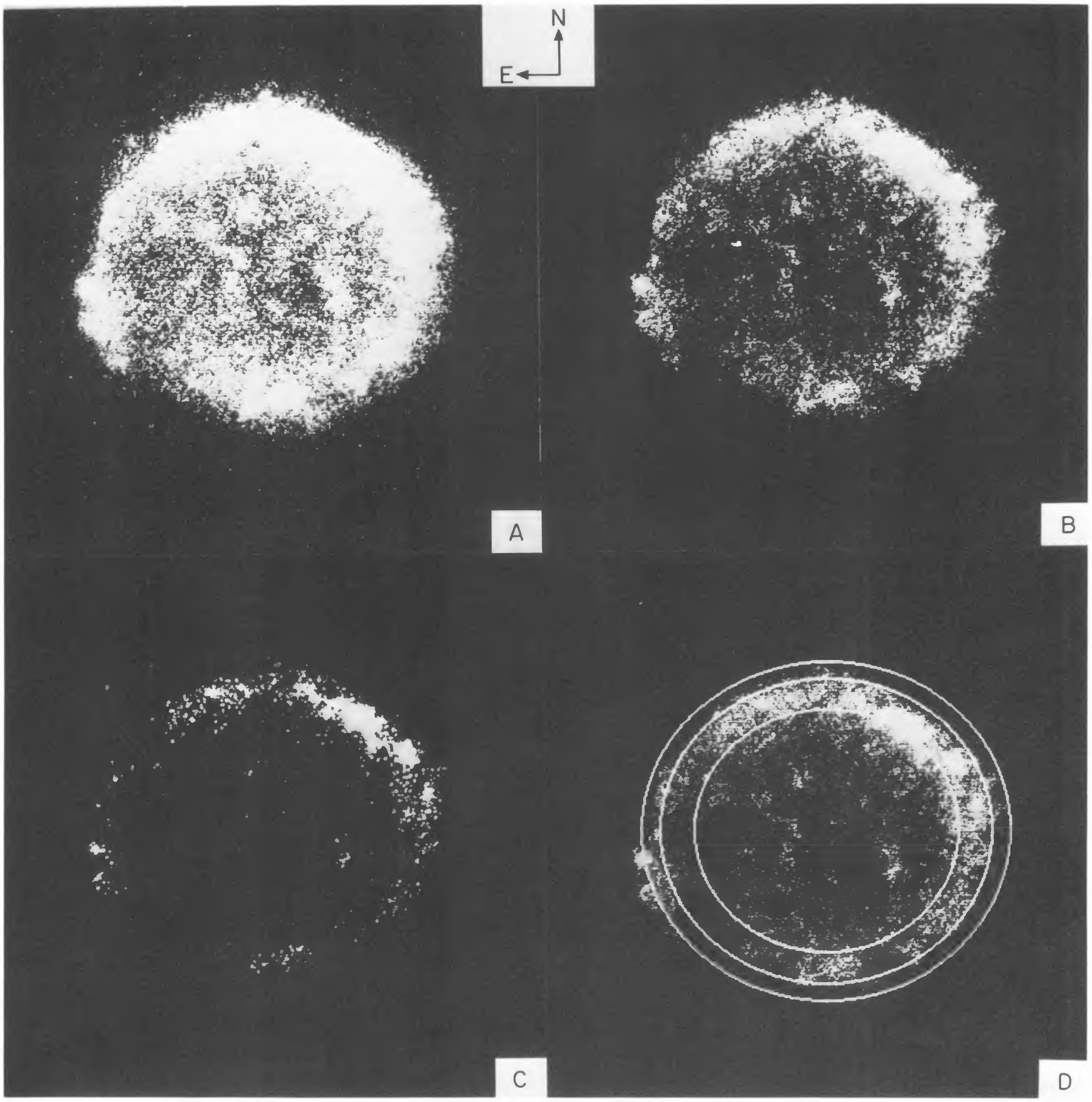

FIG. 1.—The *Einstein* HRI image of Tycho's SNR exposed to show (*a*) the faint shock heated material on the outside of the remnant, (*b*) the clumpy appearance of the X-ray emitting material, and (*c*) the brightest regions around the limb. (*d*) Circles with radii 172″, 216″, and 240″ are centered at RA $0^h22^m30^s.9$, decl. 63°51′45″. These illustrate the two shells described in the text.

systematic and model dependent uncertainties. Finally, as with most galactic SNR, the distance is not well known, and all quantitative results suffer from this uncertainty.

III. THE *EINSTEIN* HRI OBSERVATION

a) *Overview*

The *Einstein* telescope was pointed at Tycho's SNR for 22 hours starting 1940 UT, 1979 February 8. The resulting image contained 14 hours of good data and is shown in Figure 1. Several features are apparent:

1. The remnant is almost circular with diameter of 8′. There is limb brightening, not uniform around the circumference but indicative of emission from a shell, which varies from a maximum in the NW to a minimum in the SE where there is almost no limb brightening at all. There is a discontinuity in the SE which is exactly that observed in the radio region (Duin and Strom 1975; Dickel *et al.*).

2. A thin shelf of emission can be seen at the outer edge of the remnant, outside the region of maximum brightness, around most of the circumference. We assume that this feature is produced by radiation from a shock wave propagating into the interstellar medium. The interstellar shock wave is clearest on the west side and the circles shown in Figure 1*d* are centered with respect to this outer shock.

3. There is no emission detected from a central compact object or from any pointlike source within the remnant.

4. Most of the emission is from small, irregular, patchy regions. These must be clumps of material having high X-ray luminosity either because of greater than average density or greater than average emissivity. Temperature variations will also affect the brightness but not as strongly. We assume that this material is supernova ejecta. These clumps appear to be arranged inside a spherical shell (with the exception of the SE discontinuity), but the distribution within the shell is far from uniform. Individual clumps can be discerned in the center of the remnant (where we are looking approximately normal to the surface of the shell) and in the SE where the density of clumps is low. Maximum surface brightness of the remnant is in the NW, where the density of clumps is highest. The brightest regions are due to limb brightening from many overlapping high-emissivity clumps.

b) *Details*

The HRI image of a point source consists of a high resolution core FWHM $\sim 4''$ and a rather broad tail several arcminutes in extent due to scattering from imperfections in the mirrors. At 2 keV, 45% of the focused energy is contained in a circle of diameter 12″, and this fraction decreases as photon energy increases. The effect of scattering appears in the image as an increased brightness in the center of the remnant and as faint diffuse emission outside the shell. In Figure 2*a* (Plate 5), the instrument response has been deconvolved with a maximum entropy technique to remove the wings of the detector response from the image. In practice this is difficult to do exactly. The deconvolved image is somewhat sharpened, and no features appear that cannot be seen in the original data. Figure 2*b* gives a contour plot of the deconvolved image.

Figure 3 shows radial profiles of surface brightness for 12 equal segments, each spanning 30° in position angle. It illustrates the gross clumpiness in the interior of the remnant and the variation in limb brightening around the circumference. The center of these radial profiles is RA $0^h22^m30^s.9$, decl. 63°51′45″ as illustrated in Figure 1*d*. The maximum extent is exhibited by the SE discontinuity at PA 90°–120°, and the minimum extent by the adjoining region at PA 150°–180°. The shock appears in some of these profiles as a small inflection superposed on the generally smooth decrease in surface brightness going outward from maximum emission at the limb. The gradually decreasing background starting at a radius of 4′ is due to the scattering wings of the instrument response. These data were obtained from the HRI image before deconvolution. Variations in the radius of the remnant over the 30° segments, certainly over the 360° average, wash out the characteristic structure associated with the shock.

Figures 1, 2, and 3 may be compared with the IPC data given by Reid *et al.* which have a resolution of $\sim 1'$. The basic features of the remnant are the same in the IPC and in the HRI image implying that there are no gross spectral differences in emission from different parts of the remnant. The resolution of the IPC was not good enough to distinguish the shock or the clumps of material. Maximum limb brightening measured in the NW with the HRI is ≈ 4 compared with ≈ 2.5 with the IPC.

Figure 4 shows surface brightness averaged over only 10° in position angle centered at position angles of 235° and 315° (measured from N through E) where the shock is prominent. The HRI response to a uniform ring of inner and outer radii 156″ and 204″ (an approximation to the projection of a shell) is shown as a solid curve. Note that the broad wings of the HRI response to this ring (containing 90% of the emission) contribute considerable brightness over the rest of the remnant. These data are from the HRI image with no deconvolution and show the strength of the various signals and backgrounds. After subtraction of background due to instrument response to the bright limb, we calculated surface brightness of the shock and from the interior. Since densities to be calculated depend on the square root of the surface brightness, small uncertainties in background subtraction are not important.

IV. MASS DISTRIBUTION MODEL

The high-resolution image allows us to identify three components of the X-ray emission: (1) emission from an outer shell of radius $R_0 = 240''$ and thickness $\Delta R/R \sim 0.1$; this we identify with shocked interstellar matter; (2) emission from diffuse material in a shell of outer radius $R_1 \approx 216''$ and thickness $\Delta R/R \sim 0.2$; this we identify with supernova ejecta; and (3) emission from clumps

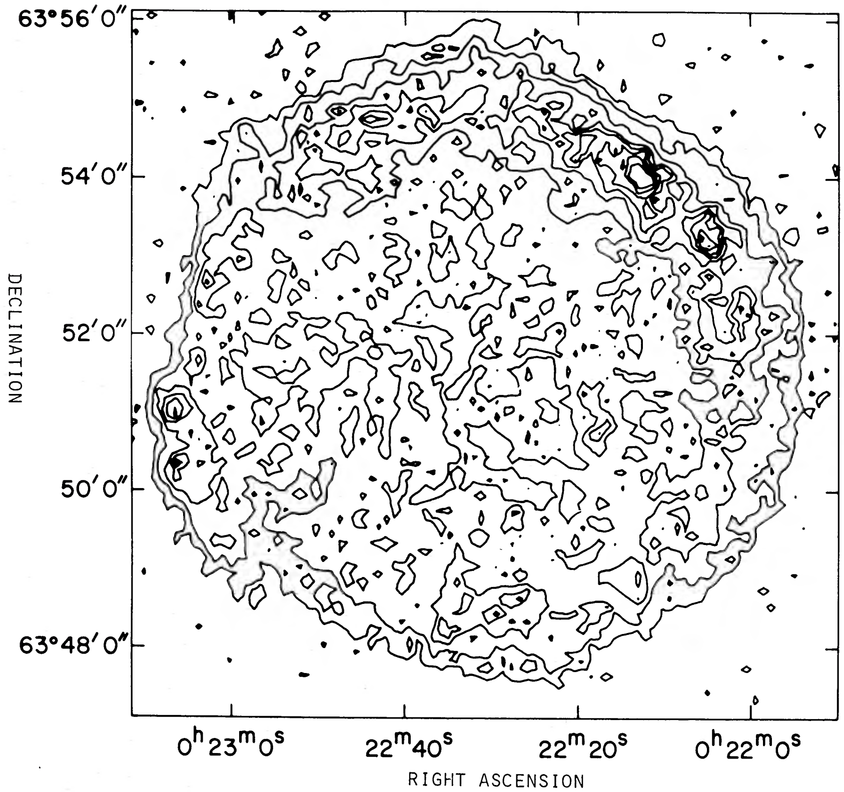

FIG. 2b.—Contour map of Fig. 2a. The spacing between the contours of constant surface brightness is 1×10^{-5} HRI counts s^{-1} $arcsec^{-2}$ except that the spacing of the first two contours is half this. Local maxima and minima in the interior cannot be identified in this figure alone. Fig. 2a must be used to distinguish between them.

distributed in the same shell as the diffuse ejecta; this we also identify with supernova ejecta. A contribution from each of these three components is summarized in Table 2.

We use the observed surface brightness of the shock to calculate the swept-up mass, M_s, and density of the ISM. We then calculate the ejecta mass, M_e, and compare the ratio of M_e/M_s with that determined from the measured dynamic state of the SNR.

The shock in the ISM is assumed to be spherical and to be composed of material of normal cosmic abundance that has been snowplowed and heated by the shock to a temperature which is dependent on the shock velocity. At the end of the next section, we will deduce a shock velocity ≈ 6000 (d/3 kpc), implying a temperature of $\approx 4 \times 10^8$ K = 36 keV. The high energy X-rays detected by Pravdo and Smith (1979) imply the existence of some high temperature material but do not support the bulk of shock heated material being at 36 keV. A lower temperature gives a better fit to the high energy spectrum, and we use a temperature of 7 keV. This is consistent with the idea that the electrons and ions have yet to come to equilibrium, so that the electron kinetic temperature is lower than the ion kinetic temperature (Itoh 1977).

TABLE 2

DATA FROM HRI IMAGE

Region	Surface Brightness (counts s^{-1} $arcsec^{-2}$)	Geometry	Signal (counts s^{-1})
Shock	7.4 (−6) at limb	shell $r_0 = 240''$ $r_i = 216''$	0.80[a]
Diffuse ejecta	0.8 (−6) at center	shell $r_0 = 216''$ $r_i = 173''$	0.21
One clump	10.3 (−6) at maximum	sphere $r = 12''$	0.0047[a]
All clumps	...	400 distributed in diffuse ejecta shell	1.86
Total remnant			2.87

[a] The tail of the detector response has been taken into account.

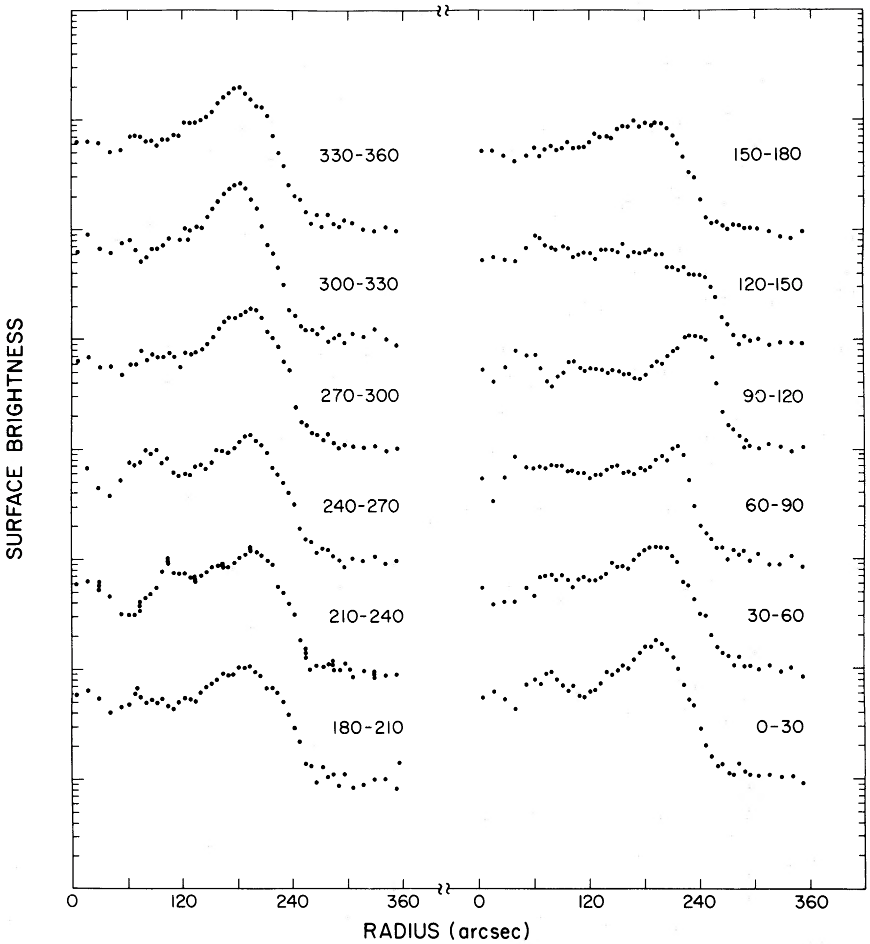

FIG. 3.—Surface brightness as function of radius at 12 different position angles

As can be seen in Figure 1, 70% of the detected X-rays come from a clumpy shell just behind the shock heated material. We assume this shell contains the stellar debris or ejecta which has been greatly enhanced in silicon group elements as required by the X-ray spectrum (Becker *et al.* 1980; Shull 1982*a*). The ejecta (or ejecta-containing regions) are clumpy, and the size distribution of clumps can be estimated from the X-ray image.

The observed clumps are not uniform, and the distribution in size can be estimated from the central part of the remnant where isolated clumps are observed. Since no unresolved point sources appear, clump dimensions can be measured. We approximate the actual distribution with two components: uniform density clumps with diameter 24″ (0.34 pc), and a uniform distribution of material filling a shell of outer radius 216″ and of thickness 0.2 of this radius.

V. CALCULATION OF SWEPT-UP AND EJECTA MASS

We take the distance to the remnant as 3 kpc. Estimates in the literature range between 2 and 6 kpc, and recent references are briefly reviewed by Strom *et al.* and Reid *et al.* The dependence of calculated mass on distance, d, is $d^{5/2}$. Thermal energy also goes as $d^{5/2}$, and kinetic energy is proportional to $d^{9/2}$.

Using the model described above (i.e., two shells of diffuse emission plus clumps), the X-ray surface brightness observations can be used to calculate density of material in the different components of the remnant. The major uncertainties in the calculation concern the emissivity of the plasma and the absorption of X-rays in the ISM between the SNR and Earth. The ISM column density is taken as 3×10^{21} atoms cm^{-2} with solar composition. This is the neutral H absorption measure of Hughes, Thompson, and Colvin (1971). The values derived from X-ray spectra are listed in Table 1 and vary greatly. The strong X-ray emission lines below 2 keV make these derivations of N_H highly uncertain. If the column density were doubled to 6×10^{21} atoms cm^{-3}, our calculated masses would increase by 30%–40%.

Considerations of ionization, recombination, and expansion time scales indicate that the ions and electrons are not in thermal equilibrium (Itoh 1977). The shock heated electrons probably achieve equilibrium, but the ions are collisionally ionized more slowly, and "ioniza-

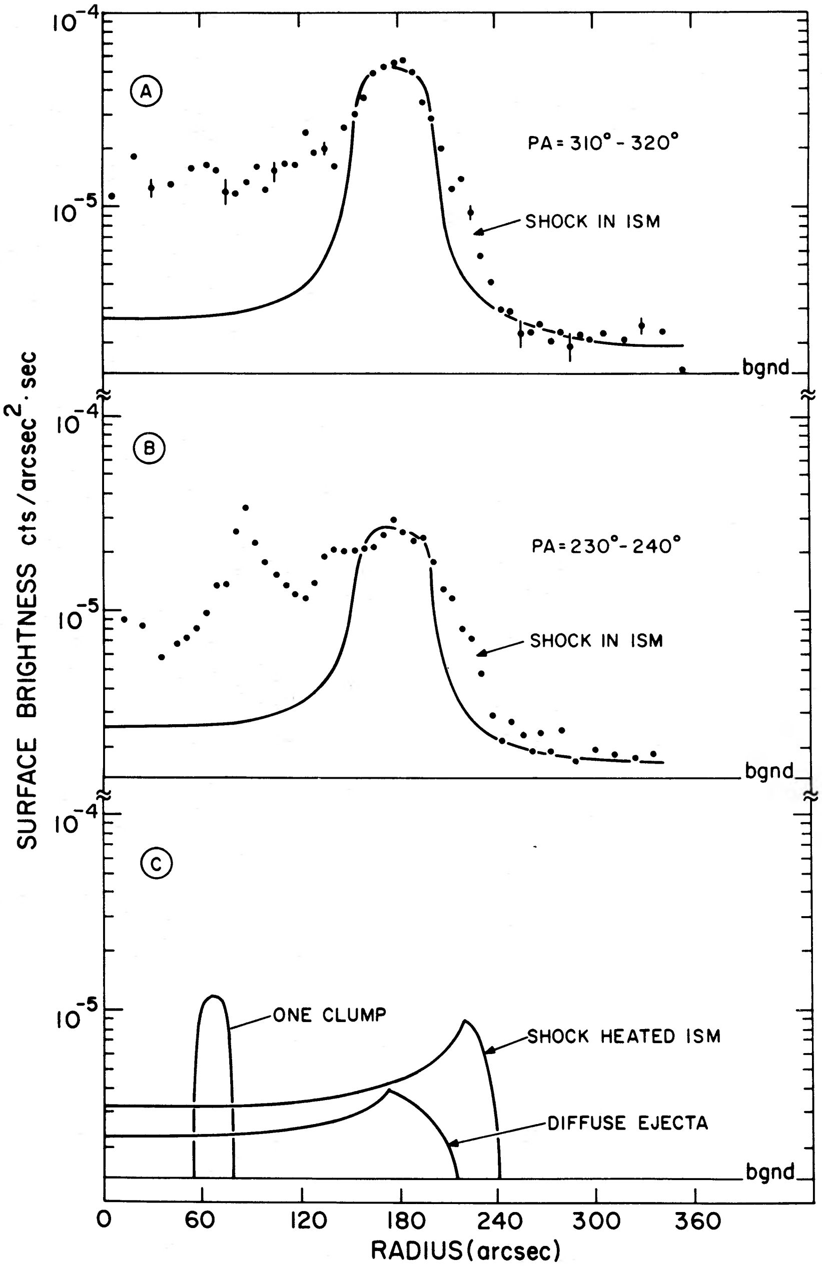

FIG. 4.—Surface brightness at two position angles (Figs. 4*a* and 4*b*), one with maximum limb brightening, one with a very bright clump. Solid curve shows instrument response to bright ring of emission. Solid curves in Fig. 4*c* show surface brightness of shell of shock heated material, inner shell of diffuse emission (as discussed in text), and of a typical clump. Lower curves refer only to source; instrument response is not included.

tion" temperature lags behind electron temperature which lags behind the ion kinetic temperature. Shull (1982*a*) has calculated the emissivity of a Sedov model for Tycho's SNR containing an enriched plasma (abundances of elements relative to solar are 0.4 [Ne], 2 [Mg], 8 [Si], 6 [S], 3 [Ar], 3 [Ca], and 2 [Fe]) and shock heated to an (electron) temperature of 7 keV. Parameters were adjusted to fit the SSS spectral data. We have used these emissivities under the assumption that emissivity of the Sedov model is approximately that of the recently shocked material. Shull (1982*b*) has also kindly provided an identical calculation for material of solar composition.

The electron density, n, in a diffuse, thin source of thermal X-rays can be calculated from the observed surface brightness using the expression

$$n^2 = 5.35 \times 10^{11} \frac{1}{H} \frac{\epsilon}{T_r P(T)} S \frac{1}{t},$$

where S is observed surface brightness in counts arcsec^{-2}

s^{-1}; t is depth of emitting region in cm; T_r is transmission of ISM and has value <1; $P(T)$ is emissivity in the 0.2–4 keV band of 1 cm^3 of plasma in ergs cm^3 s^{-1}; ϵ is detector efficiency in ergs cm^{-2} $count^{-1}$; and H is a factor, varying between 1.0 for a point source and 2.0 for a large diffuse source, which takes into account the spatial response function of the detector.

The mass, M, and X-ray luminosity, L_X, depend on the density and volume, V, of the source

$$M = \mu n V \quad \text{and} \quad L_X = n^2 P(T) V ,$$

where μ is the average ion mass per electron and n is the number of electrons cm^{-3}.

a) *Swept-up mass*

We first calculate the parameters of the interstellar shock. Subtraction of HRI background and instrument response to the bright inner ring gives the surface brightness of shocked material at the point of maximum limb brightening within the shocked ISM.

Since it is generally accepted that the gas behind the shock is not in equilibrium, we use the nonequilibrium solar calculations of Shull (1982*b*) for the emissivity. The density in the shock heated ISM is found to be 1.44 cm^{-3}. Assuming a compression factor of 3.7 behind the shock ($\Delta R/R = 0.10$), the ambient interstellar electron density is 0.39 cm^{-3}, corresponding to a baryon density $N = 0.50$ cm^{-3}. The swept-up mass is 2.2 $M_{\odot}$.

b) *Diffuse Component of Ejecta Shell*

The diffuse component of the ejecta shell is determined by the minimum measured surface brightness at the center of the remnant. There are regions in the center, apparently free of clumps, which have a residual brightness after subtraction of the HRI response to the bright regions in the rim of the remnant and subtraction of the contribution of the shocked ISM shell.

Assuming that (*a*) this material is distributed in a shell of outer radius $R_c = 216''$ and thickness $\Delta R/R = 0.2$, and (*b*) the emissivity is given by the nonequilibrium enriched calculation of Shull (1982*a*), we calculate an electron density of 0.61 cm^{-3} and a mass of 1.2 $M_{\odot}$.

If we assume that the temperatures of the electron and ion components in the diffuse shell are the same as in the swept-up material, then the pressure in the diffuse ejecta shell is less than in the shell of swept-up material, consistent with the idea that the ejecta shell is decelerating.

c) *Clumpy Ejecta*

The measured size and surface brightness of a few individual clumps were used to calculate the average characteristics of a clump. The remaining emission of the remnant, after subtracting contributions of the shock and the diffuse ejecta, was entirely assigned to clumps with no restrictions on the arrangement of the clumps within the remnant.

The density of the clumpy ejecta, assuming a nonequilibrium plasma enriched in silicon group elements, and pressure equilibrium between the diffuse and clumpy ejecta, is found to be 2.5 cm^{-3}. The mass of the clumpy ejecta is 0.7 $M_{\odot}$. Pressure equilibrium fixes the temperature of the material in clumps at 2 keV.

Table 3 summarizes the masses derived for the different components. For comparison with previous work, and to illustrate two other possibilities (which at present are not thought to be as likely as the nonequilibrium model), we have included in the table results from an equilibrium calculation with slightly enriched ejecta and superenriched ejecta.

TABLE 3

CALCULATED PHYSICAL PARAMETERS

Region	Material	Assumed Temp. (keV)	0.2–4 keV $P(T)$ (ergs cm^3 s^{-1})	n (electrons cm^{-3})	μ	Mass ($M_{\odot}$)	0.2–4 keV L_X (ergs s^{-1})
			NONEQUILIBRIUM MODEL				
Shock	Nonequilibrium solar[a]	7.0	7 (−23)	1.44	1.3	2.2	1.9 (35)
Diffuse ejecta	Nonequilibrium enriched[b]	7.0	10 (−23)	0.61	1.3	1.2	0.7 (35)
Ejecta clumps	Nonequilibrium enriched[b]	2.0	20 (−23)[c]	2.5	1.3	0.7	3.1 (35)
			IONIZATION EQUILIBRIUM MODEL				
Shock	Solar	5.0	1.2 (−23)	3.2	1.3	5.0	1.8 (35)
Diffuse ejecta	Enriched[b]	5.0	2.4 (−23)	1.15	1.3	2.3	0.6 (35)
Ejecta clumps	Enriched[b]	0.5	5.6 (−23)	4.6	1.3	1.3	3.1 (35)
			IONIZATION EQUILIBRIUM AND SUPERENRICHED EJECTA MODEL				
Shock	Solar	5.0	1.2 (−23)	3.2	1.3	5.0	1.8 (35)
Diffuse ejecta	Metal abundance 1000 × solar	5.0	2.4 (−22)	0.36	2.0	1.1	0.6 (35)
Ejecta clumps	Metal abundance 1000 × solar	0.5	2.5 (−21)	0.68	2.0	0.3	3.6 (35)

[a] Shull 1982*b*.
[b] Elemental enrichment relative to solar are: 0.4 (Ne), 2 (Mg), 8 (Si), 3 (Ar), 3 (Ca), and 2 (Fe) after Shull 1982*a*.
[c] Emissivity assumed to scale $\propto T^{-1/2}$ between 7 and 2 keV.

The ejecta mass resulting from an equilibrium calculation with temperatures derived from the SSS spectrum (Becker *et al.* 1980) is 3.6 $M_{\odot}$. The only way of reducing this mass considerably is to assume that the ejecta are bright in X-rays, not because their density is high, but because the emissivity is high. The emissivity can be increased by increasing the abundance of the medium heavy elements by a large factor. For example, if it is assumed that the medium heavy elements are enhanced by a factor of 1000, then the emissivity will be enhanced by a factor of about 10–100 depending on temperature (cf. Long, Dopita, and Tuohy 1982). The computed ejecta mass would then be reduced to 1.4 $M_{\odot}$, and the ratio of swept-up to ejected mass would be about 4.

There are two difficulties with this approach. First, if we increase the emissivity by too large a factor, then the computed density will be low, and the clumps would not be in pressure equilibrium with the surrounding gas, so it is difficult to see how they could exist. Second, if the mass of the ejecta gets too small, the SNR would be in the Sedov phase, the ejecta would be well mixed with swept-up ISM, and we would not expect to see the two-shell structure that we see. In summary, it seems that the observations of the spatial structure constrain the mass of ejecta to be approximately equal to that of the swept-up mass, and favor a nonequilibrium model in which the medium heavy abundances are enhanced only about an order of magnitude.

The nonequilibrium results given in Table 3 show that the mass of the ejecta is approximately equal to the mass of the swept-up matter. This means that Tycho's SNR is in a stage intermediate between uniform expansion and the adiabatic phase. Theoretical work on the dynamics of supernova remnants indicates that this intermediate stage is characterized by: (1) a shock wave moving into the interstellar medium with a velocity v_s (Rosenberg and Scheuer 1973); (2) a reverse shock wave moving back into the ejecta with a velocity less than v_s (MeKee 1974, Chevalier 1982*a*, *b*); and (3) clumps of material created by instabilities in the decelerating ejecta (Gull 1975; Jones, Smith, and Straker 1981).

This theoretical picture is not far from what is observed in the high resolution X-ray image of Tycho's SNR. The observed ratio of radii of the reverse and interstellar shock waves is 0.72, compared with 0.77 derived from Chevalier (1982*b*). Chevalier (1982*a*) calculates the density profile of a shock and reverse shock in a young SNR expanding into a uniform radius. Our observation is close to this, but the shocked ejecta shell is about 3 times as thick as his calculation, extending more both toward the ISM shock and back toward the center of the remnant. We attribute this to the breakup of the ejecta shell into clumps as calculated by Gull (1975) and, as expected, the size of the observed clumps is comparable with the thickness of the reversed-shocked shell.

The theoretical work is not detailed enough to satisfactorily calculate the energy and velocities from our data. Rosenberg and Scheuer (1973) calculate the propagation of a shock into a uniform ISM. By scaling Tycho's apportioned remnant to their work at $M_{\rm ej} = M_{\rm sw}$, we derive $E_0 = 1.4 \times 10^{51}$ ergs, 0.2×10^{51} ergs thermal and 1.2×10^{51} ergs kinetic. The velocity of the shock in the ISM is 6000 km s^{-1}, and the velocity of the material behind the shock as well as the contact discontinuity (the surface between the shocked ISM and the shocked ejecta) is 4500 km s^{-1}.

On the other hand, Chevalier assumes that the ISM shock velocity is $\propto t^{4/7}$ or 4700 km s^{-1} for Tycho's SNR and, at the present time ($t = 1.28t_c$ in his notation), the velocity of the reverse shock is 2700 km s^{-1}.

The expansion velocities of 3000–3600 km s^{-1} as measured by Strom *et al.* in radio and by Kamper and van den Bergh (1978) in the optical (when adjusted to a 3 kpc distance) is consistent with our analysis, assuming that these measurements refer to the shocked ejecta or preexisting material and not to the interstellar shock wave. Since most radio emission is from the region we identify with the diffuse ejecta shell (Dickel *et al.*), it is likely that the velocity of the ISM shock is considerably greater than the radio expansion velocity and that the remnant is not as close to the Sedov phase as they have concluded. The bright optical filaments are found in regions where the outermost radial contour is at a local minimum in distance from the center of Tycho's SNR. They may correspond to regions where the shock has encountered preexisting interstellar material. We suggest that the expansion velocities that are seen are those of accelerated interstellar material rather than of the primary shock. In general, we might expect the brightest and most conspicuous optical and radio filaments to occur under these local conditions and not be indicative of the higher global velocity of the interstellar shock.

The ejected mass of 1.9 $M_{\odot}$ is somewhat larger than the value of 1.4 $M_{\odot}$ expected from exploding white dwarf models (Chevalier 1981 and references therein). However, a small reduction in the assumed distance would bring the computed mass below 1.4 $M_{\odot}$, so this discrepancy is perhaps not serious. On the other hand, an increase in distance or in absorbing ISM column density will increase the mass considerably above this theoretical expectation.

VI. NO NEUTRON STAR DETECTED

Since no point sources were detected inside the remnant, we can set an upper limit to the surface temperature of a neutron star which may have been formed in the explosion. If present, this is expected at the center, but an off-center position is possible. We consider two positions: at the center where the surface brightness is low, and as a pessimistic upper limit, the bright knot $\sim 1'.5$ N of the center. The 3 σ upper limit to the signal of a point source at the center is 30 counts. If the source were located in the bright knot, the signal could be as high as 90 counts. There are several such knots or clumps inside this remnant. None appear as unresolved point sources, and there are no features which might distinguish one of them as containing a compact object.

The upper limit to the surface temperature was calculated by folding black body spectra through the

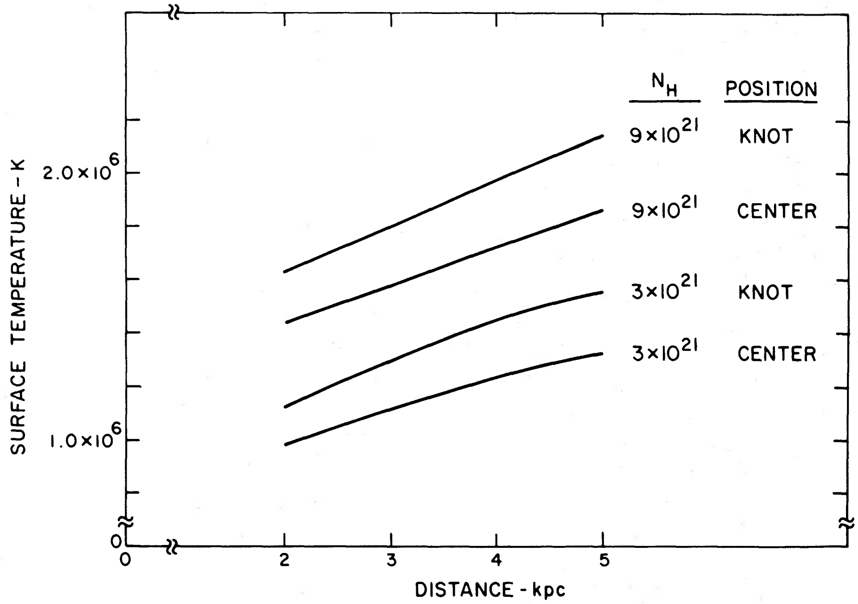

FIG. 5.—Upper limit to surface temperature (at ∞) of neutron star as a function of distance. Curves correspond to two ISM column densities and two positions within the remnant.

ISM and the detector response over a range of temperatures. Temperature is apparent temperature of the surface as observed from a great distance. The radius of the neutron star was assumed to be 11 km. The limit is also dependent on the distance and column density of ISM. Figure 5 illustrates this, and the limit ranges from 1.1×10^6 K (3 kpc most favorable observing conditions) to 1.8×10^6 K (3 kpc unfavorable observing conditions). The significance of this has been discussed at length by Nomoto and Tsuruta (1981) and by Van Riper and Lamb (1981).

VII. SUMMARY

A high resolution X-ray image of Tycho's SNR reveals three emission components: (1) an outer shell of radius 240″, $\Delta R/R \approx 0.1$; (2) a diffuse inner shell of radius 216″; and (3) ~400 bright clumps of material distributed in a shell of radius 216″, $\Delta R/R \approx 0.2$. We identify these components with (1) shocked interstellar matter, (2) diffuse supernova ejecta, and (3) clumpy supernova ejecta. The mass of these components is calculated to be 2.2 $M_\odot$, 1.2 $M_\odot$, and 0.7 $M_\odot$, respectively.

The swept-up mass is approximately equal to the ejected mass, so Tycho's SNR must be a stage intermediate between the uniform expansion and adiabatic stages. The observed morphology of the remnant is in reasonable agreement with theoretical expectations, but no numerical calculations have been published showing the reverse shock at this stage of evolution. The mass estimates scale as the distance according to $d^{5/2}$, so a reduction from the assumed distance of 3 kpc to 2.5 kpc would reduce the ejected mass to 1.4 $M_\odot$.

At a distance of 3 kpc, the upper limit on the surface temperature of a central neutron star is found to be in the range $(1.1\text{–}1.8) \times 10^6$ K.

The nonequilibrium emissivities were kindly provided by Michael Shull before publication. We thank Melanie Mitchell for calculation of the neutron star temperatures. We would also like to thank Roger Chevalier for his comments on this paper, Richard Strom for sending us the radio expansion data before publication, and Steven Murray for comments. This work was supported by NASA contract NAS 8-30751.

REFERENCES

Arnett, W. D. 1979, *Ap. J.* (*Letters*), **230**, L37.
Baade, W. 1945, *Ap. J.*, **96**, 188.
Becker, R. H., Holt, S. S., Smith, B. W., White, N. E., Boldt, E. A., Mushotzky, R. F., and Serlemitsos, P. J. 1980, *Ap. J.* (*Letters*), **235**, L5.
Chevalier, R. 1981, *Ap. J.*, **246**, 267.
———. 1982*a*, *Ap. J.*, **259**, 302.
———. 1982*b*, *Ap. J.* (*Letters*), **259**, L85.
Clark, D. H., and Stevenson, F. R. 1977, *The Historical Supernovae* (Pergamon Press, Oxford).
Dickel, J. R., Murray, S. S., and Morris, J. 1982, *Ap. J.*, **257**, 145.
Duin, R. M., and Strom, R. G. 1975, *Astr. Ap.*, **39**, 33.
Gull, S. F. 1975, *M.N.R.A.S.*, **171**, 263.
Hill, R. W., Burginyon, G. A., and Seward, F. D. 1975, *Ap. J.*, **200**, 158.
Hughes, M., Thompson, A., and Colvin, R. 1971, *Ap. J. Suppl.*, **23**, 323.
Itoh, H. 1977, *Pub. Astr. Soc. Japan*, **29**, 813.
Jones, E. M., Smith, B. W., and Straker, W. C. 1981, *Ap. J.*, **249**, 185.
Kamper, K. W., and van den Bergh, S. 1978, *Ap. J.*, **224**, 851.
Lasher, G. 1975, *Ap. J.*, **201**, 194.
Long, K. S., Dopita, M. A., and Tuohy, I. R. 1982, *Ap. J.*, **260**, 202.
Maza, J., and van den Bergh, S. 1976, *Ap. J.*, **204**, 519.
McKee, C. 1974, *Ap. J.*, **188**, 335.
Nomoto, K. 1981, in *IAU Symposium 93, Fundamental Problems in the Theory of Stellar Evolution*, ed. D. Sugimoto, D. Q. Lamb, and D. N. Schramm (Dordrecht: Reidel), p. 295.
Nomoto, K., and Tsuruta, S. 1981, *Ap. J.* (*Letters*), **250**, L19.
Oemler, A., Jr., and Tinsley, B. 1979, *A.J.*, **84**, 985.

Pravdo, S. H., and Smith, B. W. 1979, *Ap. J.* (*Letters*), **234**, L195.
Pravdo, S. H., Smith, B. W., Charles, P. A., and Tuohy, I. R. 1980, *Ap. J.* (*Letters*), **235**, L9.
Reid, P. B., Becker, R. H., and Long, K. S. 1982, *Ap. J.*, **261**, 485.
Rosenberg, I., and Scheuer, P. A. G. 1973, *M.N.R.A.S.*, **161**, 27.
Shull, J. M. 1982*a*, *Ap. J.*, **262**, 308.
———. 1982*b*, private communication.
Strom, R. G., Goss, W. M., and Shaver, P. A. 1982, *M.N.R.A.S.*, **200**, 473.
van den Bergh, S., Marscher, A. P., and Terzian, Y. 1973, *Ap. J. Suppl.*, **26**, 19.
Van Riper, K. A., and Lamb, D. Q. 1981, *Ap. J.* (*Letters*), **244**, L13.
Weaver, T. A., Axelrod, T. S., and Woosley, S. E. 1980, in *Proc. Texas Workshop on Type I Supernovae*, ed. J. C. Wheeler (Austin: University of Texas Press), p. 113.
Wheeler, J. C. 1982, in *Supernovae: A Survey of Current Research*, ed. M. J. Rees and R. J. Stoneham (Dordrecht: Reidel), in press.

P. Gorenstein, F. Seward, and W. Tucker: Harvard-Smithsonian Center for Astrophysics, 60 Garden Street, Cambridge, MA 02138

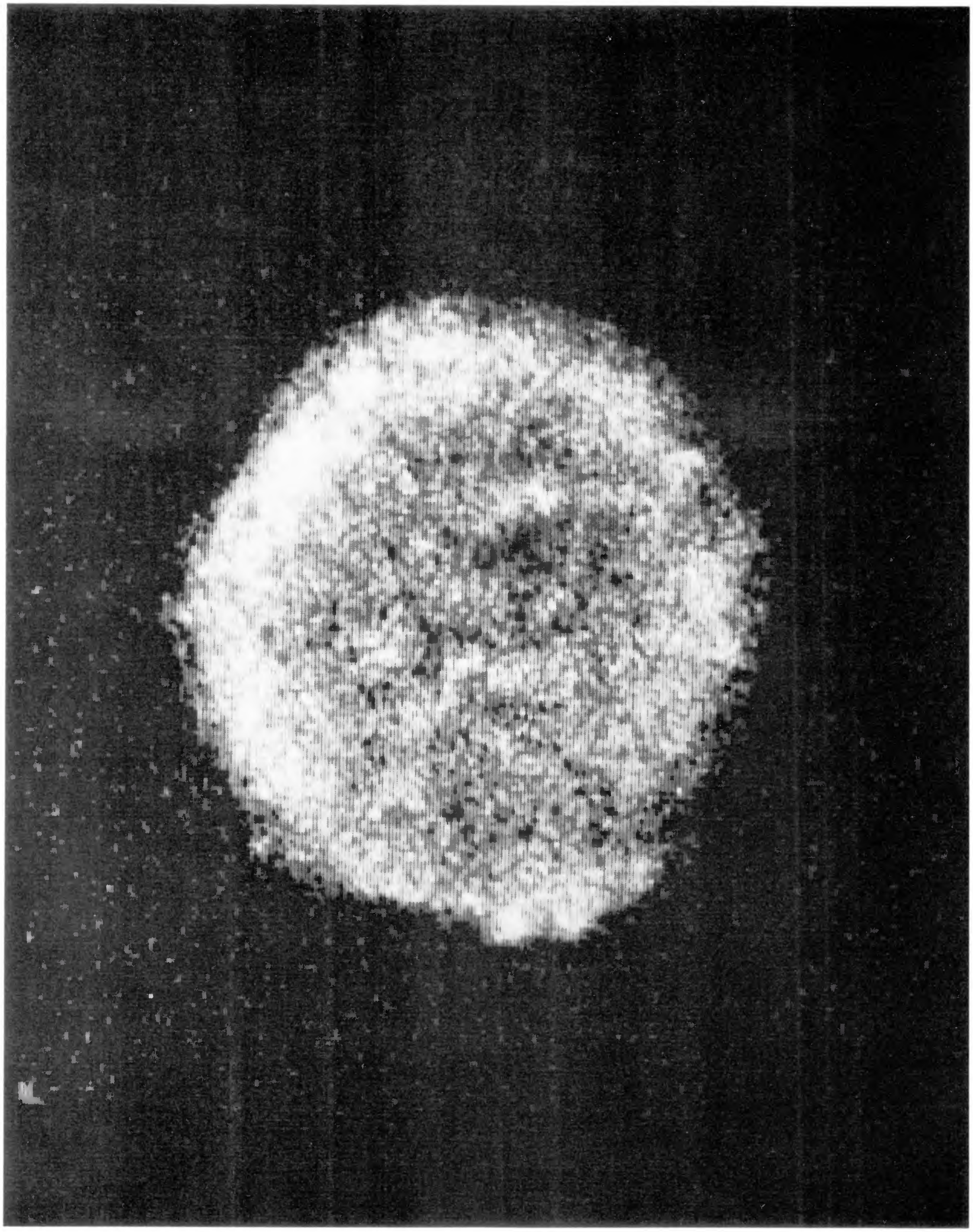

FIG. 2*a*.—Image of Tycho's SNR with instrument response deconvolved. The gray scale is logarithmic to show both faint and bright features. There is some distortion in the image display here. Spatial information should be extracted from Fig. 2*b*.

SEWARD, GORENSTEIN, AND TUCKER (*see* page 290)